



Deposited via The University of Leeds.

White Rose Research Online URL for this paper:

<https://eprints.whiterose.ac.uk/id/eprint/94446/>

Version: Accepted Version

Article:

Bonakdar, T, Ali, M, Dogbe, S et al. (2016) A Method for Grindability Testing Using the Scirocco Disperser. *International Journal of Pharmaceutics*, 501 (1-2). pp. 65-74. ISSN: 1873-3476

<https://doi.org/10.1016/j.ijpharm.2016.01.052>

© 2016. This manuscript version is made available under the CC-BY-NC-ND 4.0 license
<http://creativecommons.org/licenses/by-nc-nd/4.0/>

Reuse

Items deposited in White Rose Research Online are protected by copyright, with all rights reserved unless indicated otherwise. They may be downloaded and/or printed for private study, or other acts as permitted by national copyright laws. The publisher or other rights holders may allow further reproduction and re-use of the full text version. This is indicated by the licence information on the White Rose Research Online record for the item.

Takedown

If you consider content in White Rose Research Online to be in breach of UK law, please notify us by emailing eprints@whiterose.ac.uk including the URL of the record and the reason for the withdrawal request.

A Method for Grindability Testing Using the Scirocco Disperser

Tina Bonakdar¹, Muzammil Ali¹, Selasi Dogbe¹, Mojtaba Ghadiri^{1*}, and Arjen Tinke²

1. Institute of Particle Science and Engineering, University of Leeds, Leeds LS2 9JT, UK

*2. Janssen Research & Development, Department of Pharmaceutical Sciences – Particle & Powder
Characterization, Turnhoutseweg 30, B-2340 Beerse, Belgium*

**Contact Email: M.Ghadiri@leeds.ac.uk*

**Tel: 0044(0)1133432406*

Abstract

In the early stages of development of a new Active Pharmaceutical Ingredient (API), insufficient material quantity is available for addressing processing issues, and it is highly desirable to be able to assess processability issues using the smallest possible powder sample quantity. A good example is milling of new active pharmaceutical ingredients. For particle breakage that is sensitive to strain rate, impact testing is the most appropriate method. However, there is no commercially available single particle impact tester for fine particulate solids. In contrast, dry powder dispersers, such as the Scirocco disperser of the Malvern Mastersizer 2000, are widely available, and can be used for this purpose, provided particle impact velocity is known. However, the distance within which the particles can accelerate before impacting on the bend is very short and different particle sizes accelerate to different velocities before impact. As the breakage is proportional to the square of impact velocity, the interpretation of breakage data is not straightforward and requires an analysis of particle velocity as a function of size, density and shape. We report our work using an integrated experimental and CFD modelling approach to

evaluate the suitability of this device as a grindability testing device, with the particle sizing being done immediately following dispersion by laser diffraction. Aspirin, sucrose and α -lactose monohydrate are tested using narrow sieve cuts in order to minimise variations in impact velocity. The tests are carried out at eight different air nozzle pressures. As intuitively expected, smaller particles accelerate faster and impact the wall at a higher velocity compared to the larger particles. However, for a given velocity the extent of breakage of larger particles is larger. Using a numerical simulation based on CFD, the relationship between impact velocity and particle size and density has been established assuming a spherical shape, and using one-way coupling, as the particle concentration is very low. Taking account of these dependencies, a clear unification of the change in the specific surface area as a function of particle size, density and impact velocity is observed, and the slope of the fitted line gives a measure of grindability for each material. The trend of data obtained here matches the one obtained by single particle impact testing. Hence aerodynamic dispersion of solids by the Scirocco disperser can be used to evaluate the ease of grindability of different materials.

KEYWORDS: grindability; breakage; Scirocco; impact; aerodynamic dispersion; milling; pneumatic

1 Introduction

In the pharmaceutical, food, chemical and allied industry, including agrochemical, particles are often milled before further processing to enhance their dissolution, content uniformity in

formulations, tablet strength, etc (Rowe *et al.*, 2012). In order to specify the conditions for milling and processing in the early process development stage, it is important to be able to characterise particle grindability using the smallest possible quantity, due to the scarcity of the test material at this stage. For particles which break in the semi-brittle mode and are sensitive to strain rate, it is most appropriate to evaluate the grindability by impact testing, as it better represents the dynamics of the commonly used mills (pin mills and fluid energy mills) and also other test methods such as shearing and compression may lead to undesirable compaction.

Lecoq *et al.* (2003) designed an air jet particle impactor to study the breakage of particles of a known size distribution for a wide range of materials by impacting them on a target at a certain velocity. The concentration of particles was kept lean to minimize the particle-particle interactions. The breakage was quantified by analysing the size distribution of the impacted particles by sieving. Dumas *et al.* (2011) studied the impact breakage behaviour of precipitated silica granules using a Venturi to accelerate the particles. The particle size distribution after impact on a target was determined by laser diffraction using a Malvern Mastersizer 2000, based on which the fragmentation mechanism was analysed. Lecoq *et al.* (2011) applied the model of Vogel and Peukert (2003) to an air jet particle impactor for the determination of a particle breakage parameter. A master curve unifying the data was obtained for different materials, when the breakage parameter was plotted as a function of the applied kinetic energy to the materials. The breakage parameter in this model is based on the Weibull analysis (1988), which is an empirical fit to the experimental breakage data and is particularly applicable to the brittle failure mode. For the semi-brittle failure mode, the impact breakage of a wide range of materials has been investigated by Ghadiri and co-workers, based on which a mechanistic model of particle

chipping has been developed (Ghadiri and Zhang, 2002; Samimi *et al.*, 2003; Samimi *et al.*, 2004; Subero-Couroyer *et al.*, 2005 and Olusanmi *et al.*, 2010).

Rozenblat *et al.* (2012) carried out breakage experiments in an impact device for the development and validation of breakage models. The impact velocity of particles was obtained by a high speed digital camera. Correlations were developed for the breakage probability and breakage kernel as a function of the impact velocity and initial particle size. There is also extensive literature on the breakage and attrition of particles in high velocity air jets in which particle-particle collisions are the main mechanisms of particle breakage, e.g. Forsythe and Hertwig (1949), Gwyn (1969), Ghadiri *et al.* (1994), Ghadiri and Boerefijn (1996), Boerefijn *et al.* (2000), Bentham *et al.* (2004), Dumas *et al.* (2011), Xiao *et al.* (2012) and Zhang *et al.* (2012).

Chen and Lloyd (1994) studied the breakage of agglomerated milk powders in the dry powder dispersion unit of the Malvern Mastersizer 2600c. They found that although the device gives reliable and reproducible results for standard milk powders (non-agglomerated powders), agglomerated milk powders could break during the dispersion stage, and hence erroneous size distributions might be obtained (Boiarkina *et al.*, 2015). Rajniak *et al.* (2008) used a combination of theoretical and experimental techniques to analyse the friability of granules in pneumatic conveying systems using the Scirocco disperser of Malvern Mastersizer 2000. In a recent work by Ali *et al.* (2015), the breakage of a weak and friable spray-dried powder (burkeite) was analysed following the same approach. Their analysis suggests that the Scirocco disperser could be used as an impact breakage test device to evaluate the grindability of powders, provided the particles break in the range of achievable impact velocities with the nozzle pressures available. The advantage of using this device is that it is widely available, and dispersed particles are

presented to the laser light immediately for particle size measurement and analysis, hence reducing the time and effort required for measuring the size distribution of the impacted particles. The work reported here is focused on using this approach for a critical assessment of grindability of powders benchmarked against the single particle impact breakage method (Ghadiri and Zhang, 2002).

A schematic diagram of the Scirocco disperser is shown in Figure 1. In this device high pressured air is supplied to the air inlet (port 2), which results in a high velocity jet of air at the nozzle tip. The particles are slowly fed to the top inlet of the disperser (port 1) and get rapidly accelerated by the high velocity air jet stream. The dispersion of particles takes place as they impact at the elbow. The dispersed particles exit from the outlet (port 3) and are then presented for analysis by laser diffraction particle size measurement technique.

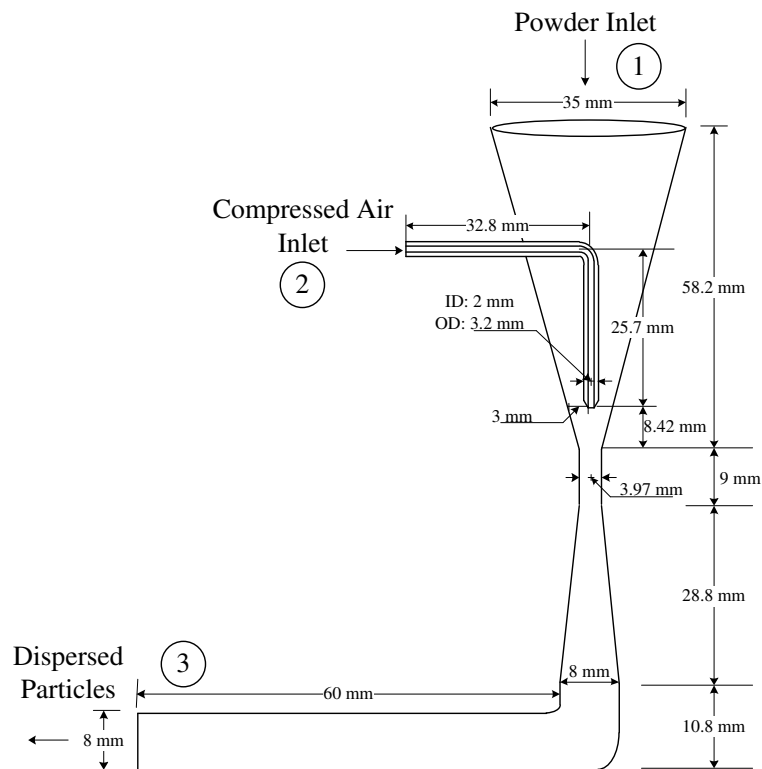


Figure 1. Schematic diagram of Scirocco disperser

In this study, narrow sieve fractions of several crystalline organic solids are dispersed in the Scirocco disperser at different pressures and the resulting particle size distributions are analysed by laser diffraction (Malvern Mastersizer 2000), from which the specific surface areas are inferred. CFD modelling of the Scirocco disperser is then carried out to evaluate the air flow distribution in the disperser. The impact velocity distributions of several particle sizes are then calculated by simulating spherical particles injected in the disperser and tracking their trajectory using a Lagrangian approach. The measured relative change of the surface area of the particles is then plotted as a function of a group representing particle characteristics and impact dynamics, with the slope of the fitted line showing a measure of grindability as an index described in the next sections. Comparing the results obtained here with the measure of the breakability obtained

from the single particle impact tester provides a quick method to evaluate grindability of different materials.

2 Methodology

The particles used in this study are crystals of aspirin, sucrose and α -lactose monohydrate (α -LM). Each material is sieved and separated into narrow size cuts: 80-90 μm , 112-125 μm , 160-180 μm and 224-250 μm for α -lactose monohydrate, 160-180 μm , 224-250 μm , 400-425 μm and 600-630 μm for sucrose, and 224-250 μm , 400-425 μm and 600-630 μm for aspirin. Each sieve fraction is then fed into the Scirocco disperser at a rate meeting the minimum obscuration requirement for particle size analysis by laser diffraction. The experiments are carried out at eight different nozzle pressures, i.e. 50, 100, 150, 200, 250, 300, 350 and 400 kPa (corresponding to 0.5, 1, 1.5, 2, 2.5, 3, 3.5 and 4 barg). The impact velocity for each sieve fraction is predicted by CFD calculations. The particle size distribution after impact is measured using the Mastersizer 2000 (Malvern Instruments, Malvern, UK) and the specific surface area (SSA) of the particles is calculated using surface mean diameter, $d_{3,2}$. In order to calculate the relative change in the specific surface area due to particle breakage, the specific surface area of the feed (SSA_0) is also required. This was taken to be the SSA obtained at the pressure of 10 kPa (0.1 barg) for each sieve fraction, thus assuming that no breakage took place at this pressure. This is actually not the case for very weak and friable materials, such as burkeite, for which SSA_0 had to be measured using the Spraytec (Malvern Instrument, Malvern, UK), where impact damage could be avoided (Ali *et al.*, 2015).

3 Predicted particle impact velocity

The air flow profiles in the disperser influence the dispersion of the particles as well as their impact velocity. Hence it is necessary to model air flow profiles to calculate the particle impact velocity. The time-averaged form of the continuity and Navier-Stokes equations are solved along with the Reynolds Stress Turbulence (RST) model for the modelling of turbulence. The time-averaged form of the continuity equation for compressible flow, assuming steady state is given by:

$$\frac{\partial}{\partial x_i}(\rho_{air} \bar{u}_i) = 0 \quad \text{Eq. (1)}$$

The time-averaged form of the Navier-Stokes equation is given by:

$$\frac{\partial}{\partial x_i}(\rho_{air} \bar{u}_i \bar{u}_j) = \frac{\partial}{\partial x_i} \left(\mu \left(\frac{\partial \bar{u}_i}{\partial x_j} + \frac{\partial \bar{u}_j}{\partial x_i} \right) \right) - \frac{\partial P}{\partial x_j} + \frac{\partial}{\partial x_i}(-\rho_{air} \overline{u_i u_j}) \quad \text{Eq. (2)}$$

The general form of the Reynolds stress transport equation is given by:

$$\underbrace{\frac{\partial}{\partial x_i}(\rho_{air} \bar{u}_k \overline{u_i u_j})}_{\text{Convective transport}} = \underbrace{P_{ij}}_{\text{Stress Production}} + \underbrace{D_{Tij}}_{\text{Diffusion}} + \underbrace{\phi_{ij}}_{\text{Pressure strain}} - \underbrace{\varepsilon_{ij}}_{\text{Dissipation}} \quad \text{Eq. (3)}$$

The convection term and stress production (P_{ij}) terms are exact. The diffusion term (D_{Tij}) is modelled via a gradient-diffusion approximation (Shir, 1973). The dissipation term (ε_{ij}) is assumed to be isotropic and is modelled in terms of the rate of dissipation of turbulent kinetic energy, which is given by:

$$\frac{\partial}{\partial x_i}(\rho_{air} \bar{u}_i \varepsilon) = \frac{\partial}{\partial x_i} \left(\left(\mu + \frac{\mu_t}{\sigma_\varepsilon} \right) \frac{\partial \varepsilon}{\partial x_i} \right) + C_{\varepsilon 1} \frac{\varepsilon}{k} G_k - C_{\varepsilon 2} \rho_{air} \frac{\varepsilon^2}{k} \quad \text{Eq. (4)}$$

The pressure strain redistribution term (ϕ_{ij}) is modelled using the linear approximation of Launder *et al.* (1975) and is modelled as the sum of the “slow” pressure strain term ($\phi_{ij,1}$), the “rapid” pressure strain term ($\phi_{ij,2}$), and the “wall reflection” term ($\phi_{ij,w}$). The pressure strain redistribution term (ϕ_{ij}) can be written as:

$$\phi_{ij} = \phi_{ij,1} + \phi_{ij,2} + \phi_{ij,w} \quad \text{Eq. (5)}$$

The slow pressure strain term $\phi_{ij,1}$, which is also known as the return to isotropy term, takes into account the effects of pressure on the Reynolds stresses. It is given by:

$$\phi_{ij,1} = -C_{\phi 1} \rho \frac{\varepsilon}{k} \left(\overline{u_i u_j} - \frac{2}{3} \delta_{ij} k \right) \quad \text{Eq. (6)}$$

The rapid pressure strain term $\phi_{ij,2}$, which is also known as the turbulence-mean flow interaction term, takes into account the effect of mean flow on the Reynolds stresses. It is given by (Launder, 1989):

$$\phi_{ij,2} = -C_{\phi 2} \left(P_{ij} - C_{ij} - \frac{2}{3} \delta_{ij} \left(\frac{1}{2} P_{kk} - \frac{1}{2} C_{kk} \right) \right) \quad \text{Eq. (7)}$$

The wall reflection term $\phi_{ij,w}$ takes into account the near wall effects on the Reynolds stresses (Gibson and Launder, 1978). It tends to damp the normal stress perpendicular to the wall and enhances the normal stress parallel to the wall. It is given by:

$$\begin{aligned} \phi_{ij,w} = & -C'_{\phi 1} \frac{\varepsilon}{k} \left(\overline{u_k u_m n_k n_m} \delta_{ij} - \frac{3}{2} \overline{u_i u_k n_j n_k} - \frac{3}{2} \overline{u_j u_k n_i n_k} \right) \frac{C_\mu^{3/4} k^{3/2}}{\kappa \varepsilon d_w} \\ & - C'_{\phi 2} \frac{\varepsilon}{k} \left(\phi_{km,2} n_k n_m \delta_{ij} - \frac{3}{2} \phi_{ik,2} n_j n_k - \frac{3}{2} \phi_{jk,2} n_i n_k \right) \frac{C_\mu^{3/4} k^{3/2}}{\kappa \varepsilon d_w} \end{aligned} \quad \text{Eq. (8)}$$

The model constants in Eqs. (4), (6), (7) and (8) are assigned the following values:

$$C_\mu = 0.09, C_{\varepsilon 1} = 1.44, C_{\varepsilon 2} = 1.92, \sigma_\varepsilon = 1.3, C_{\phi 1} = 1.8, C_{\phi 2} = 0.60, C'_{\phi 1} = 0.5, C'_{\phi 2} = 0.3$$

The near-wall flow is modelled using the standard wall functions. The discrete phase comprises particles, introduced into the disperser from the top. The trajectories of the particles are tracked using the Lagrangian approach. The equation of motion for the particles is given by:

$$\frac{d\vec{u}_p}{dt} = \vec{F}_d (\vec{u} - \vec{u}_p) + \vec{g} \quad \text{Eq. (9)}$$

The first term on the right hand side represents the drag force per unit mass and the second term represents the gravitational force per unit mass.

The drag force is given by:

$$\vec{F}_d = \frac{18\mu}{\rho_p d_p^2} \frac{C_D \text{Re}}{24} \quad \text{Eq. (10)}$$

where Re is the particle Reynolds number defined as:

$$\text{Re} = \frac{\rho_{air} d_p |\vec{u}_p - \vec{u}|}{\mu} \quad \text{Eq. (11)}$$

The correlation for the drag coefficient (C_D) for particles proposed by Morsi and Alexander (1972) is used, which is applicable to smooth spherical bodies. The effect of the fluctuating velocities of air on the particle dispersion is taken into account using the discrete random walk model (Hutchinson *et al.*, 1971). The particle-particle interaction is ignored in the simulation.

The coupling between the air and particles is one way, i.e. the air flow influences the trajectories of particles but the momentum exerted by the particles on the gas phase is ignored. This assumption is valid for flows involving a lean concentration of particles, i.e. solids volume fractions less than 10^{-6} (Loth et al., 2005). This is the case for the experimental work carried out here. The particle velocity is primarily influenced by the mean air velocity, which is not expected to change appreciably due to a lean concentration of particles. The restitution coefficient (defined as the ratio of rebound to incident particle velocities) is assumed to be 0.5 for all the sizes and for all the materials considered.

The conservation equations for the continuous and discrete phases in three-dimensions are solved using the CFD software Fluent v. 12 (2009), which utilises the finite volume discretisation method for the governing equations. The meshing of the disperser is carried out using Gambit (2006). The selected mesh comprised of 4.1×10^5 tetrahedral and hexahedral cells. The second-order upwind discretisation scheme (Versteeg and Malalasekera, 1995) was used for the convective terms. For the pressure-velocity coupling the SIMPLE scheme (Versteeg and Malalasekera, 1995) was used, and for the pressure interpolation, the second-order scheme was used.

For the inlet nozzle boundary condition, a pressure inlet is specified at the face of the air nozzle with values varying for different cases. A pressure outlet with a value of 0 kPa (0 barg) is specified at the outlet face. To enable the entrainment of air from the top of the disperser, where the particles are introduced, a pressure outlet boundary condition is specified at the top with a value of 0 kPa (0 barg). For the turbulence boundary conditions, a turbulence intensity of 5% at the corresponding faces of the inlet and exit ports are specified. The inlet pressures considered

are: 50, 100, 150, 200, 250, 300, 350 and 400 kPa (corresponding to 0.5, 1, 1.5, 2, 2.5, 3, 3.5 and 4 barg). The spherical particle diameters considered for prediction of the impact velocity are: 170 μm , 237 μm , 412 μm and 615 μm , corresponding to the geometric mean of the sieve cuts 160-180 μm , 224-250 μm , 400-425 μm and 600-630 μm , respectively. To obtain a statistically reliable particle impact velocity distribution when they impact at the elbow of the disperser, 200 particles were injected from a circular area with 10 mm diameter at the centre of the powder inlet face (port 1 in Figure 1).

The convergence criteria for the continuity, momentum and Reynolds stresses were specified as 1×10^{-4} and for the energy equation, it was 1×10^{-6} . The residuals converged to the required tolerance limit for the cases in which the inlet pressure was from 50 kPa to 250 kPa (0.5 barg to 2.5 barg). However, at 300 kPa (3 barg) inlet pressure, the residuals did not converge to the required tolerance level. For this case, the simulation was considered to have converged when the residuals did not reduce any further after reaching a certain level.

Figures 2-4 are plots of the average impact velocity of all the materials considered as a function of the inlet air pressure. The average impact velocity is calculated by taking the mean of the impact velocity of all the particles upon the first impact with the elbow, which was found to be the highest particle-wall impact velocity compared to other secondary collisions with the wall.

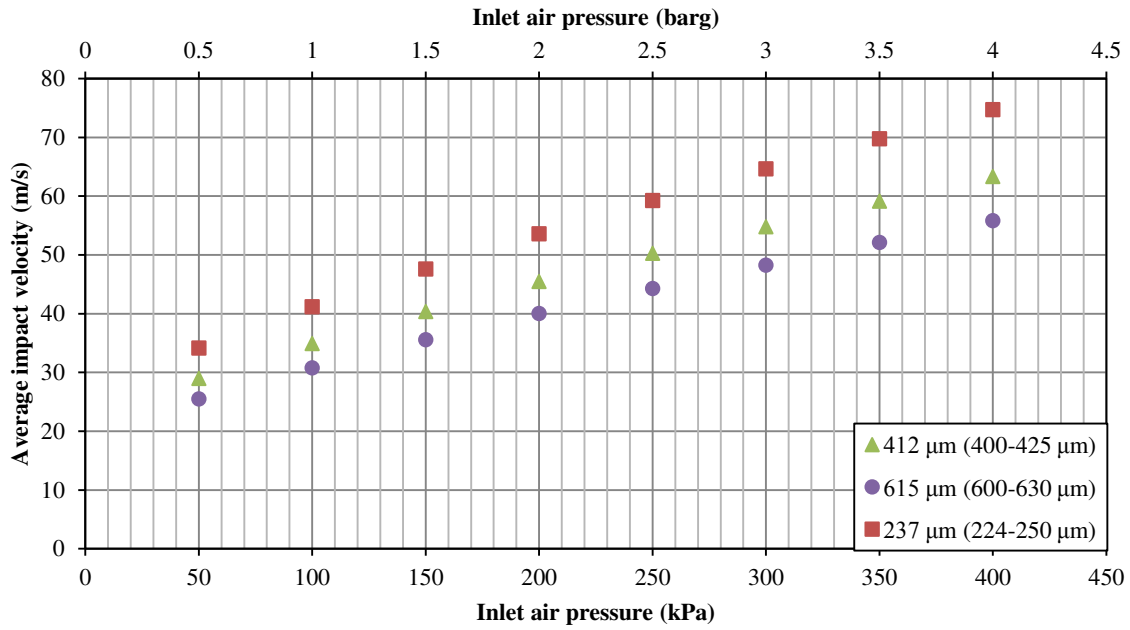


Figure 2. Average impact velocity of particles as a function of nozzle air pressure for aspirin

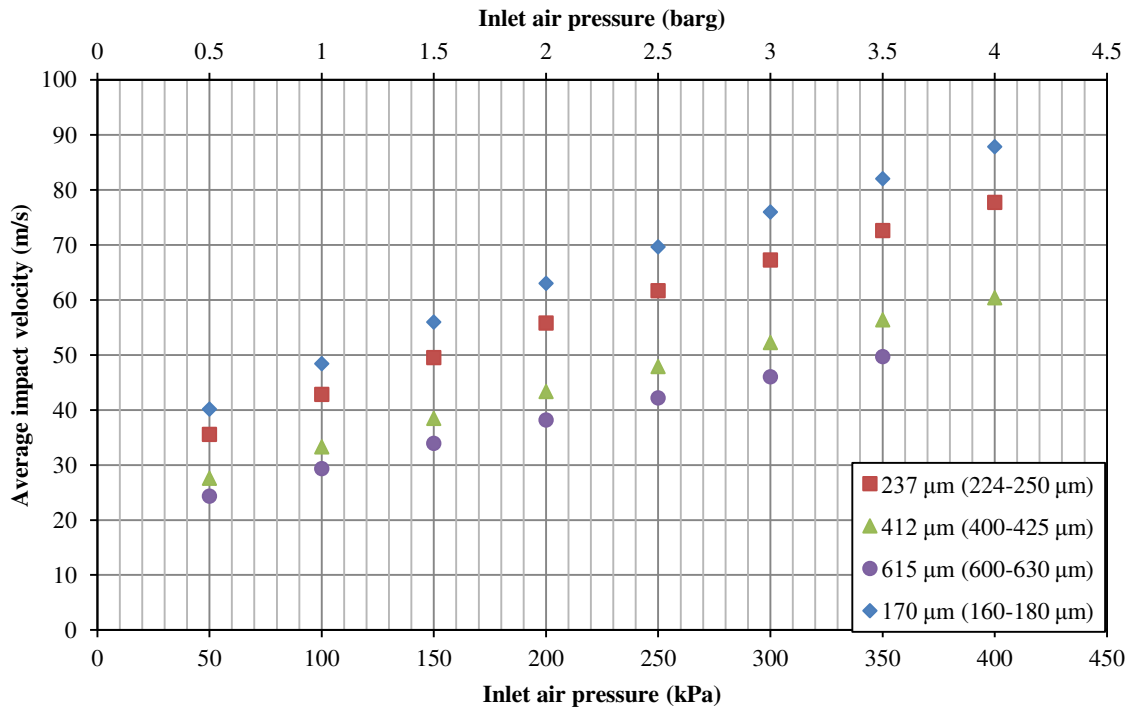


Figure 3. Average impact velocity of particles as a function of nozzle air pressure for sucrose

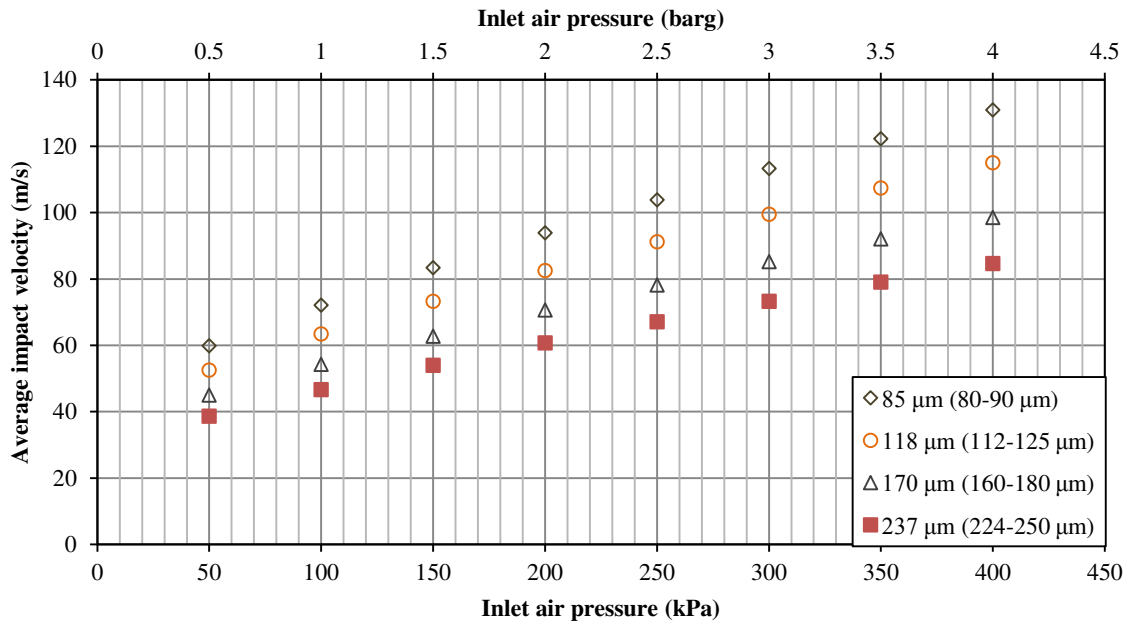


Figure 4. Average impact velocity of particles as a function of nozzle air pressure for α -lactose monohydrate

Qualitatively all the test materials show a similar trend, i.e. with increasing pressure, the impact velocity of the particles is increased. The smaller particles accelerate faster due to lower momentum and attain a higher impact velocity than the larger ones. Comparing Figures 2-4, for a given inlet nozzle pressure and particle size, the small variation of impact velocity for the test materials arises from differences in their density. The rate of rise of impact velocity with the nozzle pressure is initially linear, but it slows down at higher pressures.

4 Experimental results and discussion

Particle impact velocity in the Scirocco L-bend depends on particle size. Therefore narrow sieve sizes of the test materials were prepared using a combination of British Standard and DIN sieve sizes. Each sieve fraction was fed into the Scirocco disperser of Malvern Mastersizer 2000 and

the particle size distribution was analysed. A sensitivity analysis was carried out to find out the optimum vibratory feed rate as well as the minimum mass required to provide an adequate obscuration (2-4%), whilst ensuring minimal interparticle interactions. In the work carried out here the volume fraction of solids fed to the disperser was roughly 6×10^{-7} , in line with the lean phase requirement for comparison with simulation results. Using a very small mass quantity is one of the advantages of using the Scirocco disperser to evaluate the grindability of the particles, as the sample quantity could be a critical issue (i.e. 1-2 g depending on the particle size).

The particle size distributions of aspirin, sucrose and α -lactose monohydrate particles for the feed size of 224-250 μm , having passed through the Scirocco at different nozzle pressures, are shown in Figures 5-7 as typical examples. The rest of data for all sieve fractions are shown in the appendix.

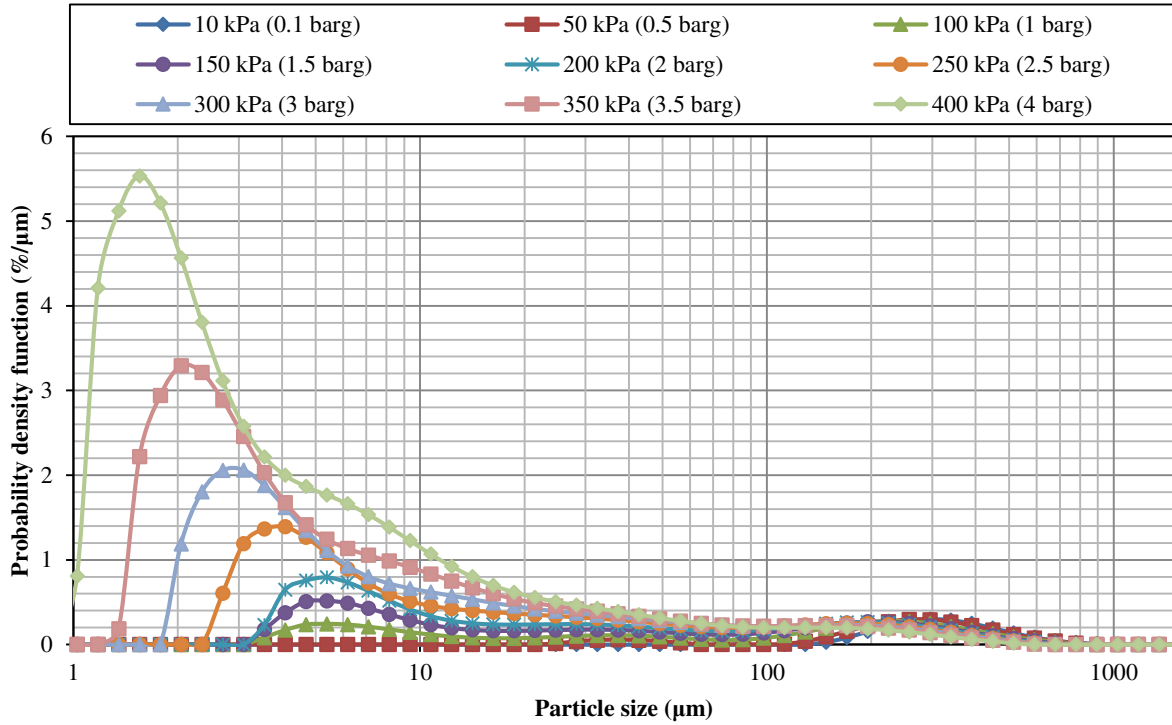


Figure 5. Relative shift in size distribution of 224-250 μm of aspirin at different nozzle pressures

Despite particles having a narrow size distribution, laser diffraction gives a relatively large span, e.g. referring to the case of aspirin in Figure 5, we get a range from nearly 150-600 μm for the size 224-250 μm (see 0.1 barg). The data for 50 kPa (0.5 barg) almost overlap with 10 kPa (0.1 barg), without much breakage. The formation of debris first appears at 100 kPa (1 barg), which leads to bimodal particle size distribution. As the nozzle pressure increases the average size of debris decreases. The higher air pressures give rise to larger impact velocities in the Scirocco disperser, shifting the particle size distributions to the left.

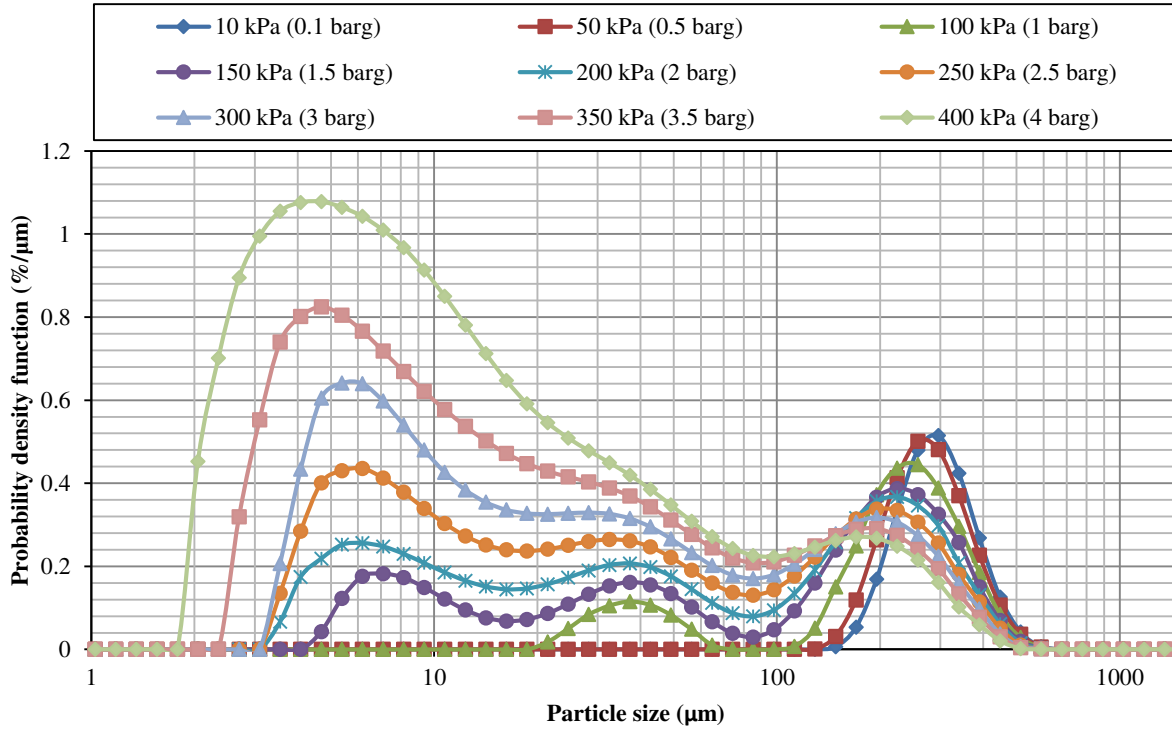


Figure 6. Relative shift in size distribution of 224-250 μm of sucrose at different nozzle pressures

For sucrose, 50 kPa (0.5 barg) gives some fragments with a slight shift to smaller sizes compared to 10 kPa (0.1 barg). The formation of debris is observed at 100 kPa (1 barg). Increasing the nozzle pressure then leads to a shift in particle size distribution to the left. The average diameter of debris produced during the tests decreases as the nozzle pressure increases. Comparing Figures 5 and 6 shows that for the same nozzle pressure and feed size of materials, aspirin particles tend to break more than sucrose particles.

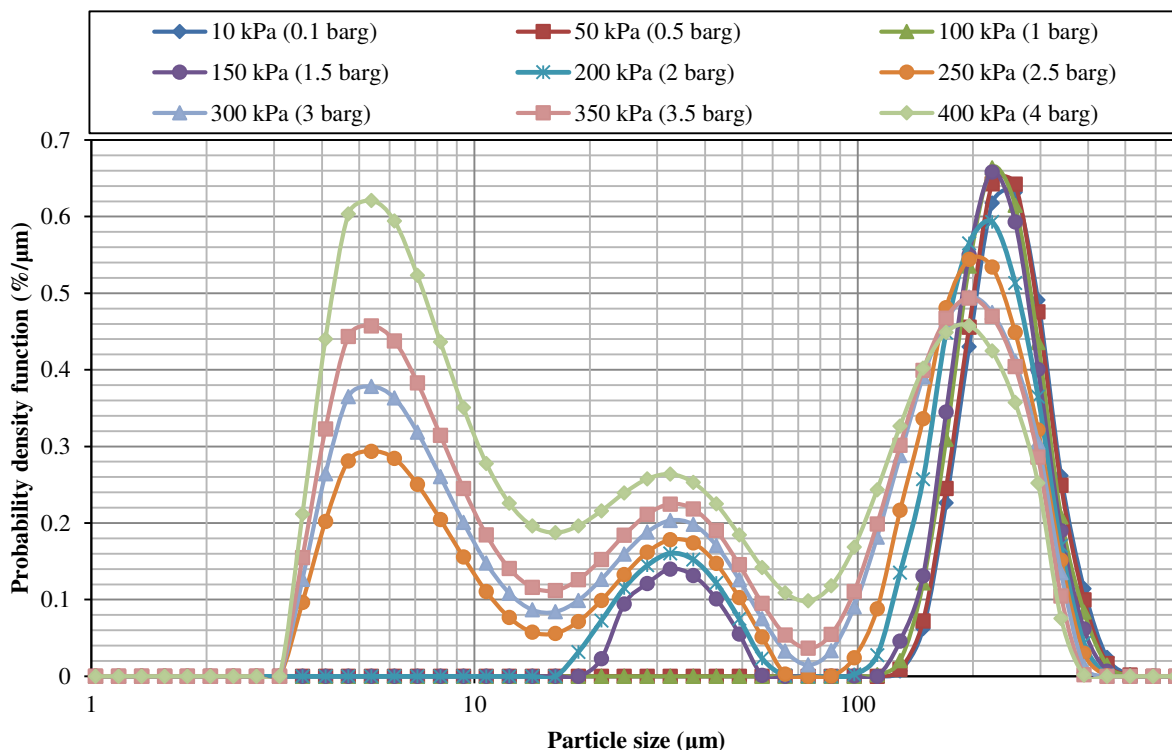


Figure 7. Relative shift in size distribution of 224-250 μm of α -lactose monohydrate at different nozzle pressures

For lactose, 50 kPa (0.5 barg) almost overlaps with 10 kPa (0.1 barg). A slight shift in particle size distribution to the left and formation of fragments are observed for 100 kPa (1 barg). The formation of debris occurs at higher pressures (150 kPa), compared to the two other test materials. More debris with smaller sizes are produced when the nozzle pressure is increased. Comparison of Figures 5-7 shows that, at a constant nozzle pressure, aspirin breaks more than sucrose, and sucrose breaks more than lactose for a given particle size.

5 Analysis of particle breakage

The first impact in the elbow of the Scirocco disperser, for which the velocity is the highest, is considered to be responsible for particle breakage. The specific surface area of the particles

reported by the Malvern Mastersizer 2000 at different impact velocities is used to calculate the shift in the specific surface area, ΔSSA . This is normalised with respect to the initial specific surface area, SSA_0 (relative shift) and plotted as a function of impact velocity for the test materials as shown in Figures 8-10:

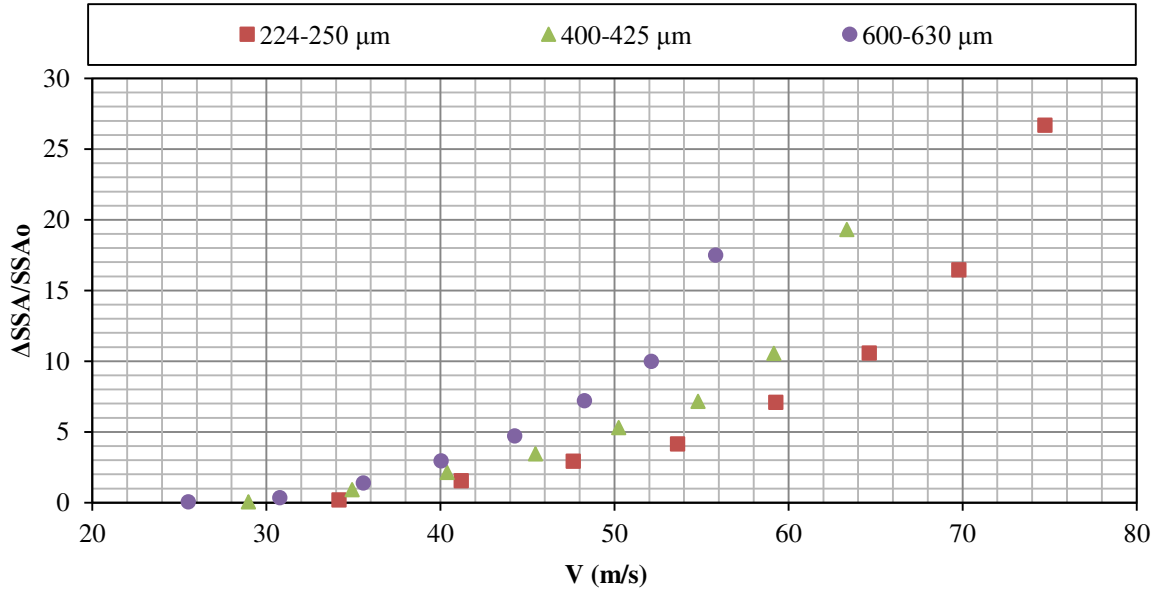


Figure 8. Relative shift in the specific surface area of aspirin as a function of impact velocity in Scirocco disperser

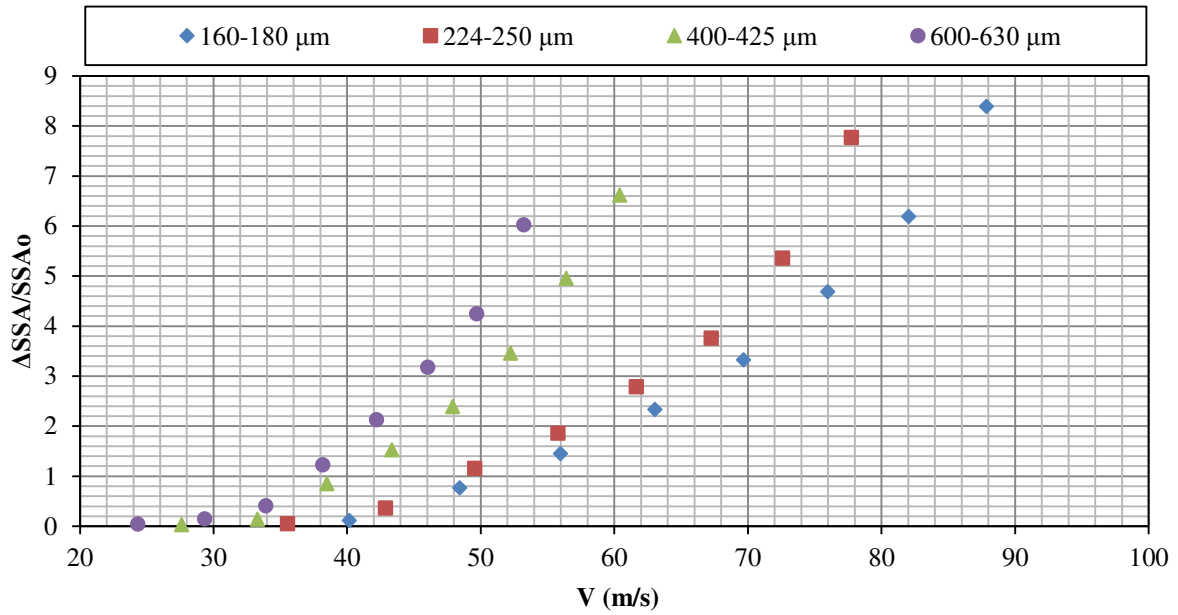


Figure 9. Relative shift in the specific surface area of sucrose as a function of impact velocity in Scirocco disperser

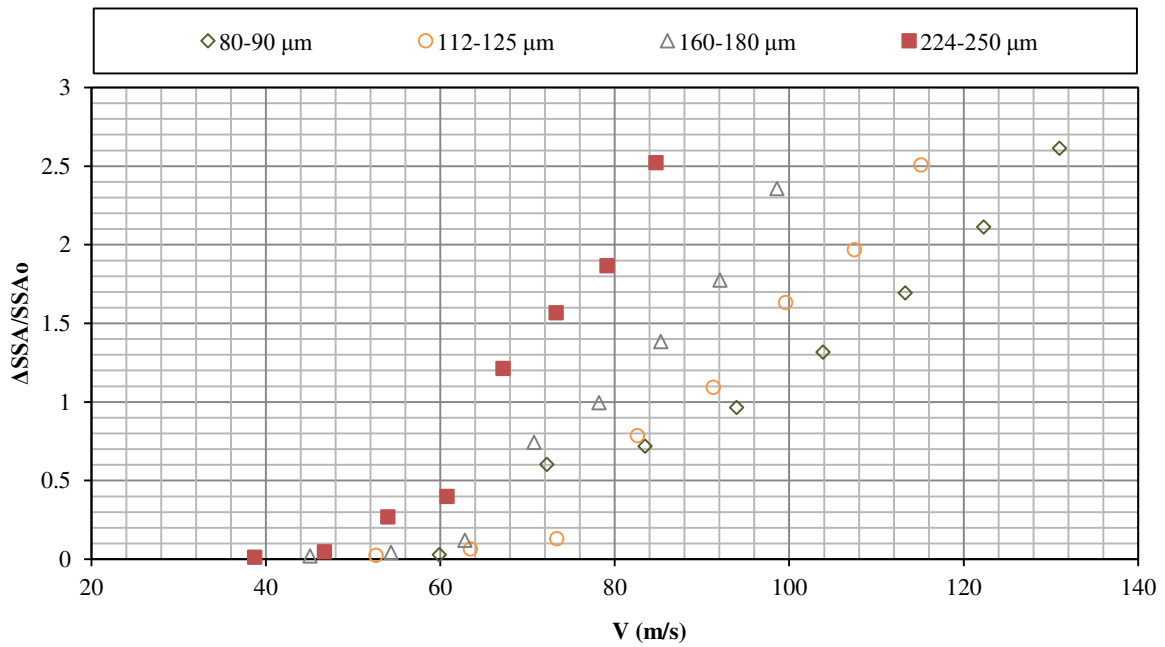


Figure 10. Relative shift in the specific surface area of α-lactose monohydrate as a function of impact velocity in Scirocco disperser

A family of curves is observed for all the test materials with clear trends for the effect of impact velocity and particle size. At a constant impact velocity, the larger particle sizes tend to break more than the smaller ones.

The test materials used here all fail through the semi-brittle failure mode (Olusanmi *et al.*, 2010), i.e. crack propagation is preceded by plastic flow of the impact site. We therefore use the model of Ghadiri and Zhang (2002) for the analysis of impact breakage as shown below:

$$R^* = \alpha\eta = \alpha \frac{\rho_f d_{f,v}^3 H}{K_c^2} V^2 = C \rho_f d_{f,v} V^2 \quad \text{Eq. (12)}$$

where R^* is the extent of breakage, expressed on a gravimetric basis, describing the mass fraction of debris obtained experimentally and η is a dimensionless group representing the breakage propensity of the semi-brittle materials. $d_{f,v}$ is a measure of feed particle size (on a volumetric basis), ρ_f is the envelope density of feed particles and V is their impact velocity. The parameter C ($\alpha H/K_c^2$) is a lumped parameter describing the mechanical properties of the material, in which α , H and K_c represent proportionality factor, hardness and fracture toughness of the material, respectively.

R^* is expressed on a gravimetric basis, but using the Malvern Mastersizer 2000, the particle size distribution is characterised by laser diffraction and expressed on a volumetric basis. So it is necessary to relate the shift in particle size distribution to R^* . As the breakage process could produce a wide size distribution, it is more convenient to express R^* in terms of the relative change in the specific surface area. This approach has been presented by Ali *et al.* (2015) and is adopted here for the analysis of breakage of aspirin, sucrose and α -lactose monohydrate in the

Scirocco disperser. Considering the definition of R^* , the mass fraction of debris can be expressed by Eq. (13)

$$R^* = \alpha\eta = \frac{n_d \rho_d \left(\frac{\pi}{6} \bar{d}_{d,v}^3\right)}{n_f \rho_f \left(\frac{\pi}{6} \bar{d}_{f,v}^3\right)} \quad \text{Eq. (13)}$$

where ρ_f and ρ_d are the densities of feed particles and debris, respectively. n_f and n_d are the numbers of feed particles and debris, respectively. $\bar{d}_{f,v}$ is the average size (volumetric basis) of the feed material, and $\bar{d}_{d,v}$ is the average size of the debris, which is calculated based on the particle size distribution after Scirocco testing, as qualitatively shown in Figure 11 and described below. The size distribution of the debris is obtained from the shaded area, from which the volume-weighted arithmetic mean size, $\bar{d}_{d,v}$, and the relative shift in the specific surface area ($\Delta SSA / SSA_0$) are calculated.

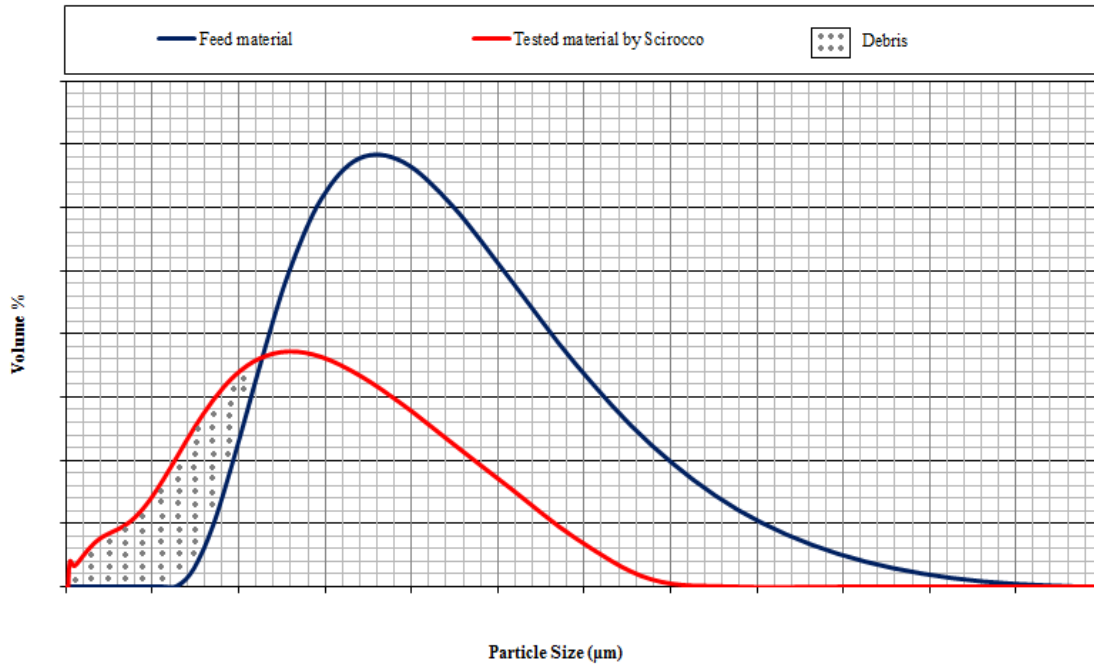


Figure 11. Calculation of debris size distribution based on the distribution of feed and broken materials

Conversion of Eq. (13) to a surface area basis requires $\bar{d}_{f,v}$ and $\bar{d}_{d,v}$ to be expressed in terms of surface-area equivalent diameters. This can be done by the use of the sphericity shape factor, ψ , defined as the ratio of the surface area of the volume-equivalent sphere (πd_v^2) to the actual particle surface area, S : $n_d \bar{d}_{d,v}^2 = \psi_d S_d$ and $n_f \bar{d}_{f,v}^2 = \psi_f S_f$. Therefore we get

$$\frac{\rho_d \bar{d}_{d,v}}{\rho_f \bar{d}_{f,v}} \times \frac{\psi_d S_d}{\psi_f S_f} = \alpha \eta \quad \text{Eq. (14)}$$

where S_d and S_f are the surface area of debris and feed material, respectively. ψ_d and ψ_f are the sphericity shape factor of debris and feed particles, respectively. The ratio S_d/S_f represents the relative shift in the surface area, i.e.

$$\frac{S_d}{S_f} = \frac{\Delta SSA}{SSA_0} \quad \text{Eq. (15)}$$

where ΔSSA is the specific surface area of debris.

Therefore by converting the extent of breakage (gravimetric basis) to the relative shift in the surface area, we get

$$\alpha \frac{\rho_f \bar{d}_{f,v} V^2 H}{K_c^2} \times \frac{\rho_f \bar{d}_{f,v}}{\rho_d \bar{d}_{d,v}} \times \frac{\psi_f}{\psi_d} = \frac{\Delta SSA}{SSA_0} \quad \text{Eq. (16)}$$

The characterisation of the ratio of sphericity of feed material to debris requires extensive work.

In the first instance this is considered as a constant. Hence Eq. (16) can be presented as below:

$$\beta \frac{\rho_f \bar{d}_{f,v} V^2 H}{K_c^2} \times \frac{\rho_f \bar{d}_{f,v}}{\rho_d \bar{d}_{d,v}} = \frac{\Delta SSA}{SSA_0} \quad \text{Eq. (17)}$$

where β is a new proportionality factor corresponding to $\alpha \frac{\psi_f}{\psi_d}$.

The relative shift in the specific surface area can now be plotted as a function of $\rho_f \bar{d}_{f,v} V^2 \left(\frac{\rho_f \bar{d}_{f,v}}{\rho_d \bar{d}_{d,v}} \right)$ for all the three test materials as shown in Figure 12. For crystalline solids, the envelope density is not expected to change as particles undergo size reduction, so $\rho_d = \rho_f$. It should be noted that for porous particles, such as the spray-dried particles analysed by Ali *et al.* (2015), this is not the case and the density ratio has to be evaluated.

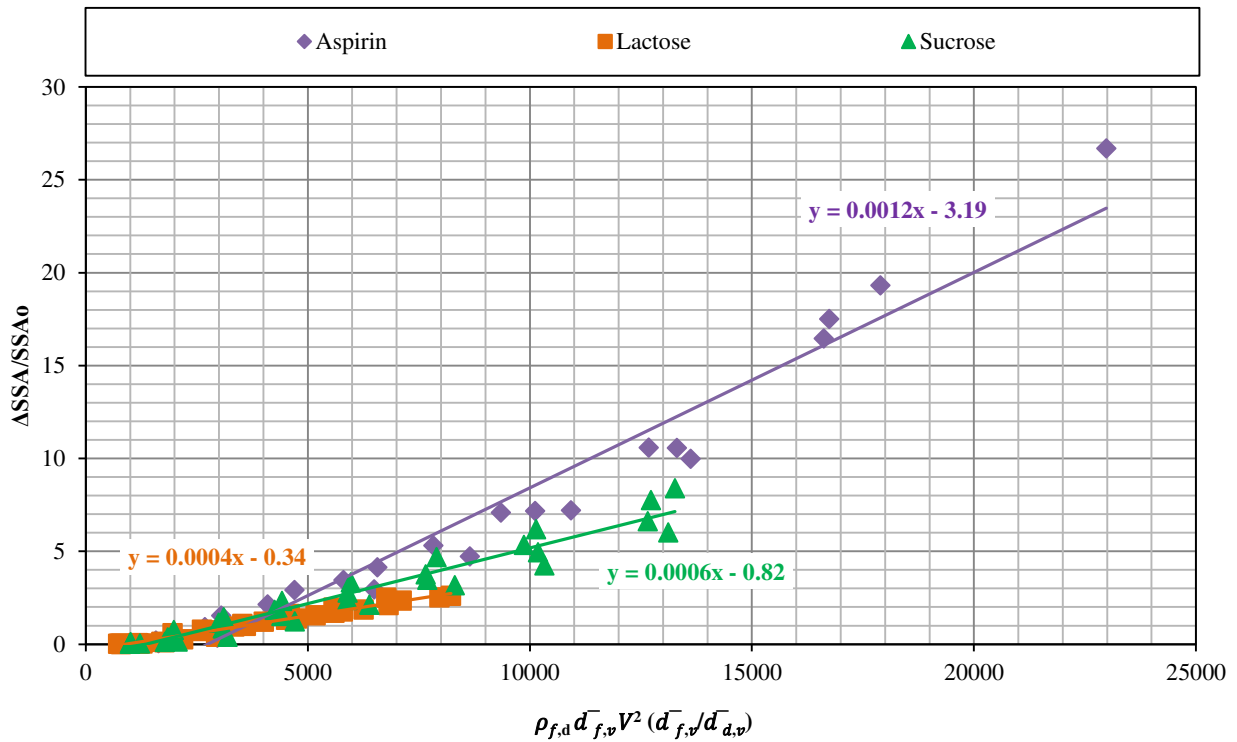


Figure 12. Shift in the specific surface area of aspirin, sucrose and lactose particles as a function of $\rho_f \bar{d}_{f,v} V^2 \left(\frac{\bar{d}_{f,v}}{\bar{d}_{d,v}} \right)$

For each test material a good unification of breakage data is obtained for the particle sizes and inlet nozzle pressures tested. Moreover, the slope of the lines, $\beta H/K_c^2$, reflect the ease with which the particles break in the Scirocco disperser, and is thus expected to correlate with similar

data obtained by the single particle impact breakage method, provided interparticle interaction in the Scirocco disperser does not affect the rate of breakage. Furthermore, the intercept of each line gives the impact velocity for a given particle size below which the particles would not break. This provides a design rule for mitigating particle breakage in pneumatic conveying lines.

6 Single particle impact breakage parameter

Experiments have been carried out by various research workers in the past in which $\alpha H/K_c^2$, the breakability index, of Eq. (12) has been determined from the slope of the line of R^* as a function of $\rho_f \bar{d}_{f,v} V^2$ (Ali *et al.*, 2015). The material mechanical properties of aspirin, sucrose and α -lactose monohydrate have been obtained using the same approach. The most recent analysis is summarised in Table 1.

Table 1. Material properties of aspirin, sucrose and α -lactose monohydrate

Material	Density (kg/m ³)	$\alpha H/K_c^2$
Aspirin	1397	0.050
Sucrose	1587	0.026
α -LM	1520	0.017

The slopes of the two lines of particle breakage obtained by Scirocco testing and from single particle impact testing, as given in Figure 12 and Table 1, should be correlated as they both

reflect the impact damage. The larger they are, the easier the particles break. Therefore the ratio of the slopes for the same set of materials should be comparable. This is shown in Table 2.

Table 2. The ratio of slopes for each two materials obtained from single particle impact testing and Scirocco testing

Material	Ratio of slopes from single particle impact testing	Ratio of slopes from Scirocco testing
<i>Aspirin/Sucrose</i>	1.9	2.0
<i>Sucrose/Lactose</i>	1.5	1.5
<i>Aspirin/Lactose</i>	2.9	3.0

In summary, a very good match is observed between the ratio of mechanical properties obtained by the Scirocco disperser and by the single particle impact tester. The ratios show the ease of breakability of one material compared to another. For instance, the ratio of the slopes for sucrose to α -lactose monohydrate is 1.5, which shows that sucrose can be milled 1.5 times easier than α -lactose monohydrate. This information can be used to evaluate the grindability of different materials. Considering that the mass required to be tested in the Scirocco is very low, the method is attractive for cases where the sample supply is scarce, e.g. new active pharmaceutical ingredients in the pharmaceutical industry.

7 Conclusions

An experimental study of particle breakage integrated with a CFD analysis of particle impact in the Scirocco disperser has been carried out to evaluate its suitability as a grindability test device.

The impact velocities of three test materials, i.e. aspirin, sucrose and α -lactose monohydrate, for a range of particle sizes have been calculated for eight nozzle pressures. The impact velocity of particles increases almost linearly initially with increasing the nozzle pressure, but the rate of increase slows down at high pressures.

The relative increase in the specific surface area of the particles, with respect to the initial value following impact in the Scirocco disperser, shows a linear dependence on $\rho_f \bar{d}_{f,v} V^2 \left(\frac{\bar{d}_{f,v}}{\bar{d}_{d,v}} \right)$. The slope of the fitted line reflects the particle breakage propensity and correlates well with $\alpha H/K_c^2$, obtained by single particle impact testing. Therefore this method can be used to evaluate the grindability of powders and grains, provided the particle impact velocity is first determined.

8 Acknowledgements

The authors are grateful to Drs Paul Kippax and Fraser McNeil-Watson for information on the Scirocco design and to Dr Colin Hare for his suggestion to use the narrowest possible size distribution of each test to reduce data scatter due to size effect. This was achieved by using a combination of British Standard and DIN sieve sizes. We also like to thank Michiel Van Nyen on Stagier training at Janssen Research and Development, Beerse, Belgium for his assistance in particle size analysis.

References

Ali, M., Bonakdar, T., Ghadiri, M. and Tinke, A. (2015). Particle breakage in a scirocco disperser. *Powder Technology*. Vol. 285: 138-145

Bentham, A.C., Kwan, C.C., Ghadiri, M. and Boerefijn, R. (2004). Fluidised bed jet milling of pharmaceutical powders. *Powder Technology*, vol. 141, pp. 233-238

Boerefijn, R., Gudde, N.J. and Ghadiri, M. (2000). A review of attrition of fluid cracking catalyst particles. *Advanced Powder Technology*, vol. 11, pp. 145-174.

Boiarkina, I., Sang, C., Depree, N., Yu, W., Young, B. R. and Wilson, D. I. (2015). Significance of powder breakdown during in-plant transport at industrial milk powder plants. *APCCChE 2015 Congress incorporating Chemeca 2015*, Melbourne, Victoria.

Chen, X. D. and Lloyd, R.J. (1994). Some aspects of measuring the size and rate of dispersion of milk powder agglomerates using the Malvern Particle Sizer 2600c. *Journal of Dairy Research*, vol. 61, pp. 201-208.

Dumas, T., Bonnefoy, O., Grosseau, P., Thomas, G., Nebut, S. and Guy, L. (2011). New methods to analyse fragmentation mechanisms of precipitated silicas. *5th International Workshop on Granulation, Granulation Conference Lausanne*, Switzerland.

Fluent User's guide. *Ansys Inc.* 2009.

Forsythe, W. L. and Hertwig, W. R. (1949). Attrition characteristics of fluid cracking catalysts. *Ind. Eng. Chem.*, vol. 41, pp. 1200-1206.

Gambit, (2006). version 2.4, <http://www.ansys.com>

Ghadiri, M. and Boerefijn, R. (1996). A Model of Attrition in the Jetting Region of Fluidised Beds. *KONA Powder and Particle*, No. 14, pp. 5-15.

Ghadiri, M., Cleaver, J.A.S., Tuponogov, V.G. and Werther, J. (1994). Attrition of FCC Powder in the Jetting Region of a Fluidised Bed. *Powder Technology*, vol. 80, pp. 175-178.

Ghadiri, M., and Zhang, Z. (2002). Impact attrition of particulate solids. Part 1: A theoretical model of chipping. *Chemical Engineering Science*, vol. 57, pp. 3659-3669.

Gibson, M. M. and Launder, B. E. (1978). Ground effects on Pressure fluctuations in the atmospheric boundary layers. *J. Fluid Mech.*, vol. 86, part 3, pp. 491-511.

Gwyn, J. E. (1969). On the particle size distribution function and the attrition of cracking catalysts. *AIChE J.*, vol. 15, pp. 35-39.

Hutchinson, P., Hewitt, G. F. and Dukler, A. E. (1971). Deposition of liquid or solid dispersions from turbulent gas streams: a stochastic model. *Chemical Engineering Science*, vol. 26, pp. 419-439.

Launder, B. E. (1989). Second moment closure and its use in modelling turbulent industrial flows. *Int. J. Numer. Meth. Fl.*, vol. 9, pp. 963-985.

Launder, B. E., Reece, G. J. and Rodi, W. (1975). Progress in the development of a Reynolds stress turbulence closure. *J. Fluid Mech.*, vol. 68, part 3, pp. 537-566.

Lecoq, O., Chamayou, A., Dodds, J. A. and Guigon, P. (2011). Application of a simplifying model to the breakage of different materials in an air jet mill. *Int. J. Miner. Process.*, vol. 99, pp. 11-16.

Lecoq, O., Chouteau, N., Mebtoul, M., Large, J. F. and Guigon, P. (2003). Fragmentation by high velocity impact on a target: a material grindability test. *Powder Technology*, vol. 133, pp. 113-124.

Loth, E., Tryggvason, G., Tsuji, Y., Elghobashi, S., Crowe, C., Berlemont, A., Reeks, M., Simonin, O., Frank, T., Onishi, Y. and Wachem, B. (2005). Modeling. In: C. Crowe, ed., *Multiphase Flow Handbook*, 1st ed. London: CRC.

Morsi, S. A. and Alexander, A. J. (1972). An investigation of particle trajectories in two-phase flow systems. *J. Fluid Mech.*, vol. 55 (2), pp. 193-208.

Olusanmi, D., Wang, C., Ghadiri, M., Ding, Y. and Roberts, K.J., 2010, "Effect of temperature and humidity on the breakage behaviour of Aspirin and sucrose particles", *Powder Technology*, 201(3), 248-252.

Rajniak, P., Dhanasekharan, K., Sinka, C., MacPhail, N. and Chern, R. (2008). Modeling and measurement of granule attrition during pneumatic conveying in a laboratory scale system. *Powder Technology*. Vol. 185: 202-210

Rowe, R., Sheskey, P., Cook, W., 2012. Handbook of Pharmaceutical Excipients: Edited by Raymond C. Rowe, BPharm, PhD, DSC, FRPharmS, FRSC, CPhys, MInstP, Chief Scientist, Paul J.

Rozenblat, Y., Grant, E., Levy, A., Kalman, H. and Tomas, J. (2012). Selection and breakage functions of particles under impact loads. *Chemical Engineering Science*, vol. 71, pp. 56-66.

Samimi A., Ghadiri, M., Boerefijn, R., Groot, A., Kohlus, R. , 2003, "Effect of structural characteristics on impact breakage of agglomerates", *Powder Technology*, 130, pp. 428-435.

Samimi, A., Moreno, R., Ghadiri, M. , 2004, "Impact damage analysis of agglomerates: effect of impact angle", *Powder Technology*, 143-4, pp. 97-109.

Shir, C. C. (1973). A preliminary numerical study of atmospheric turbulent flows in the idealized planetary boundary layer. *J. Atm. Sci.*, vol. 30, pp. 1327-1339.

Subero-Couroyer, C., Ghadiri, M., Brunard, N., Kolenda, F. , 2005, "Analysis of catalyst particle strength by impact testing: The effect of manufacturing process parameters on the particle strength", *Powder Technology*, 160(2), 67-80.

Versteeg, H. K. and Malalasekera, W. (1995). *An Introduction to Computational Fluid Dynamics*. Longman Scientific and Technical, Harlow.

Vogel, L. and Peukert, W. (2003). Breakage behaviour of different materials – construction of a mastercurve for the breakage probability. *Powder Technology*, vol. 129, pp. 101-110.

Weichert, R. (1988). Correlation between probability of breakage and fragment size distribution of mineral particles. *International Journal of Mineral Processing*, 22 (1), pp. 1-8.

Xiao, G., Grace, J. R. and Lim, C. J. (2012). Limestone particle attrition in high-velocity air jets. *Ind. Eng. Chem. Res.*, vol. 51, pp. 556-560.

Zhang, Q., Jamaledine, T. J., Briens, C., Berruti, F. and McMillan, J. (2012). Jet attrition in a fluidized bed. Part I: Effect of nozzle operating conditions. *Powder Technology*, vol. 229, pp. 162-169.

Appendix

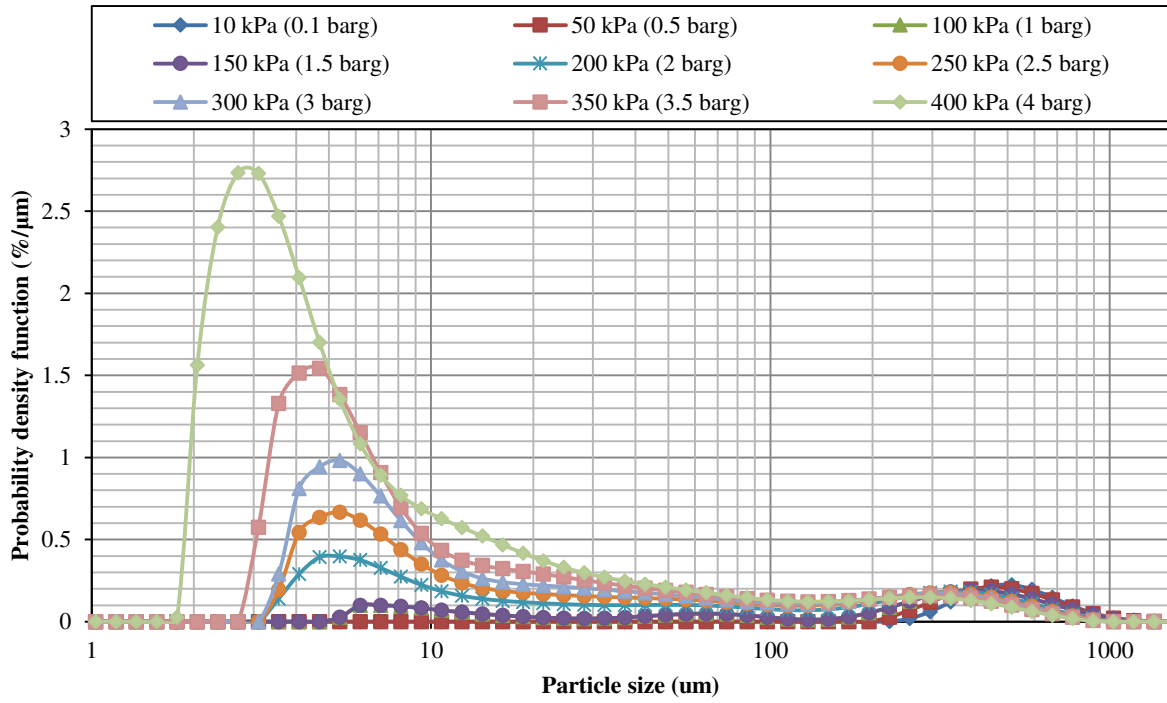


Figure a1: Shift in size distribution of 400-425 μm of aspirin at different nozzle air pressures

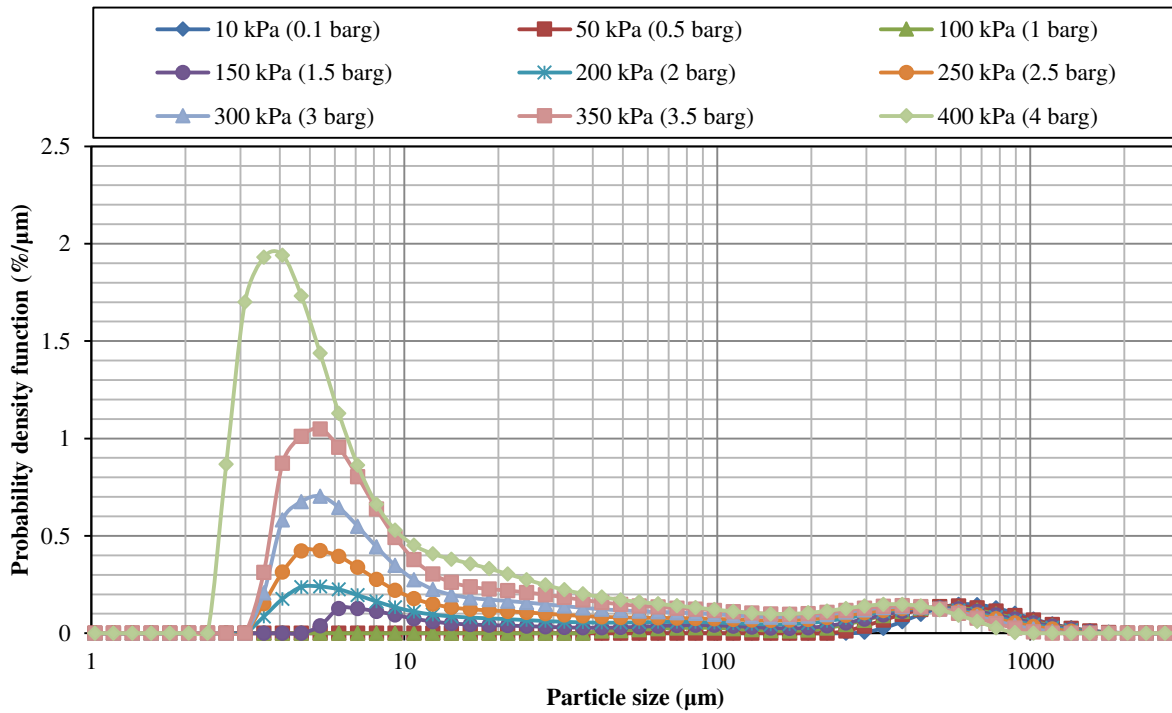


Figure a2: Shift in size distribution of 600-630 μm of aspirin at different nozzle air pressures

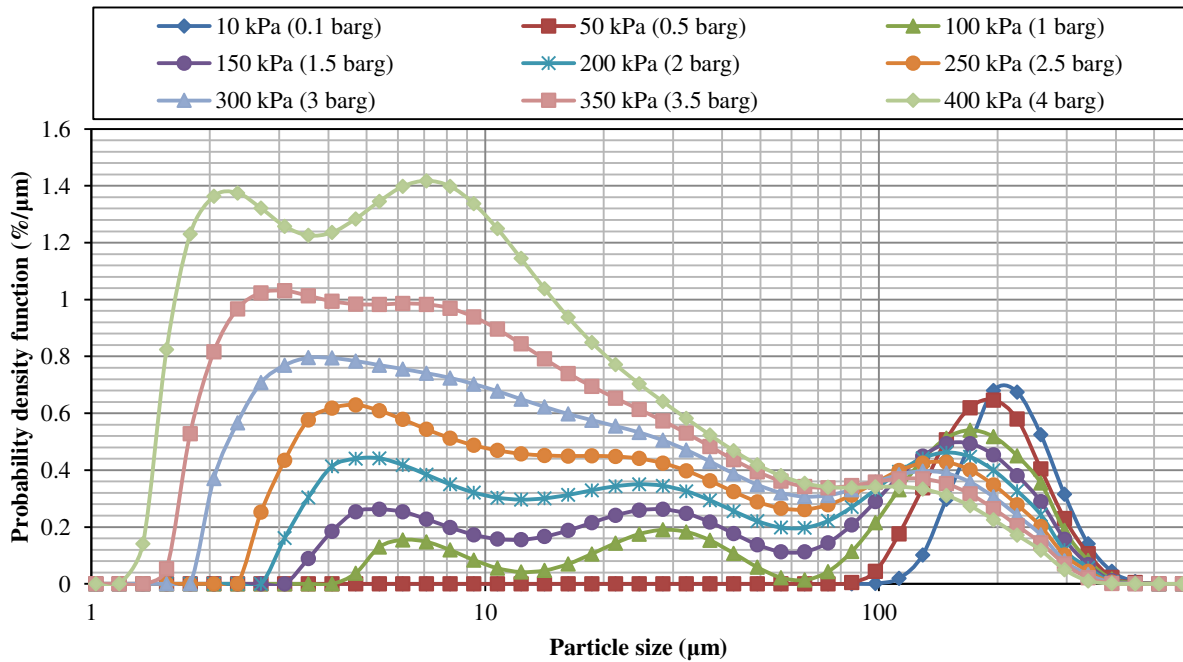


Figure a3: Shift in size distribution of 160-180 μm of sucrose at different nozzle air pressures

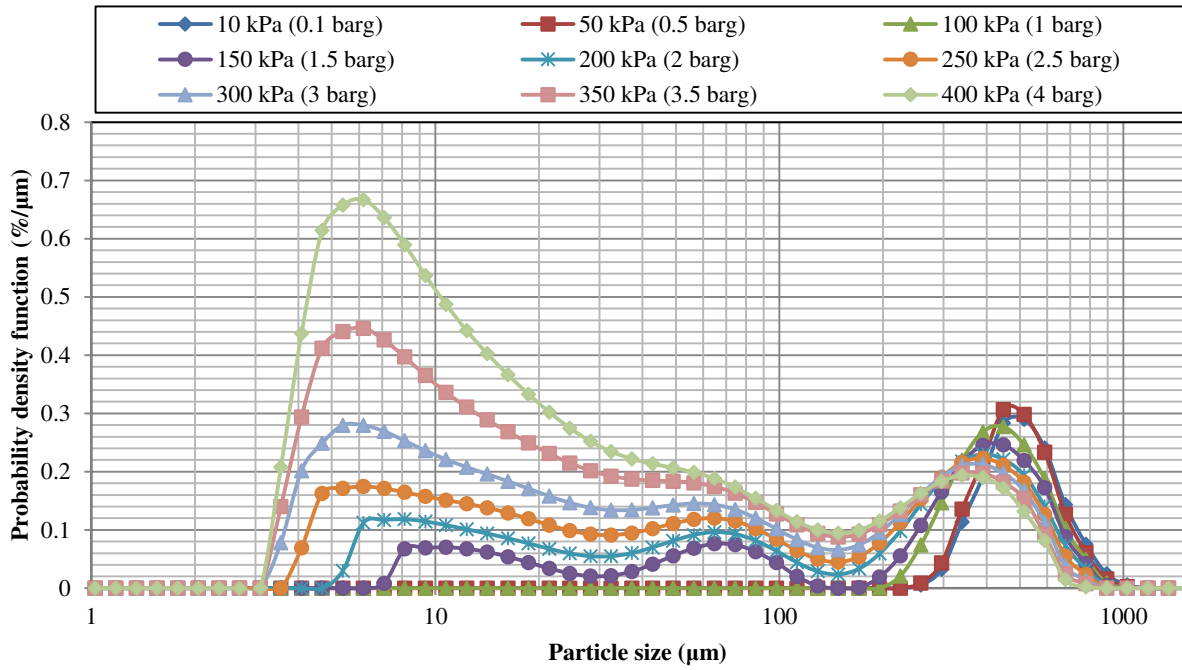


Figure a4: Shift in size distribution of 400-425 μm of sucrose at different nozzle air pressures

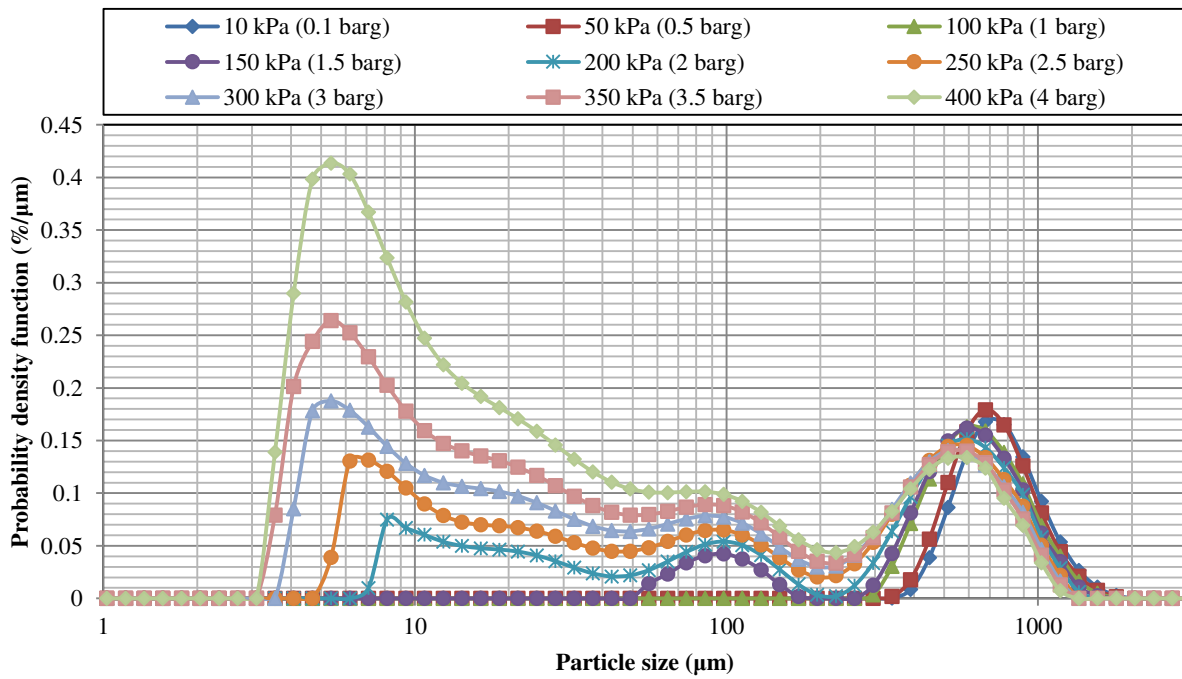


Figure a5: Shift in size distribution of 600-630 μm of sucrose at different nozzle air pressures

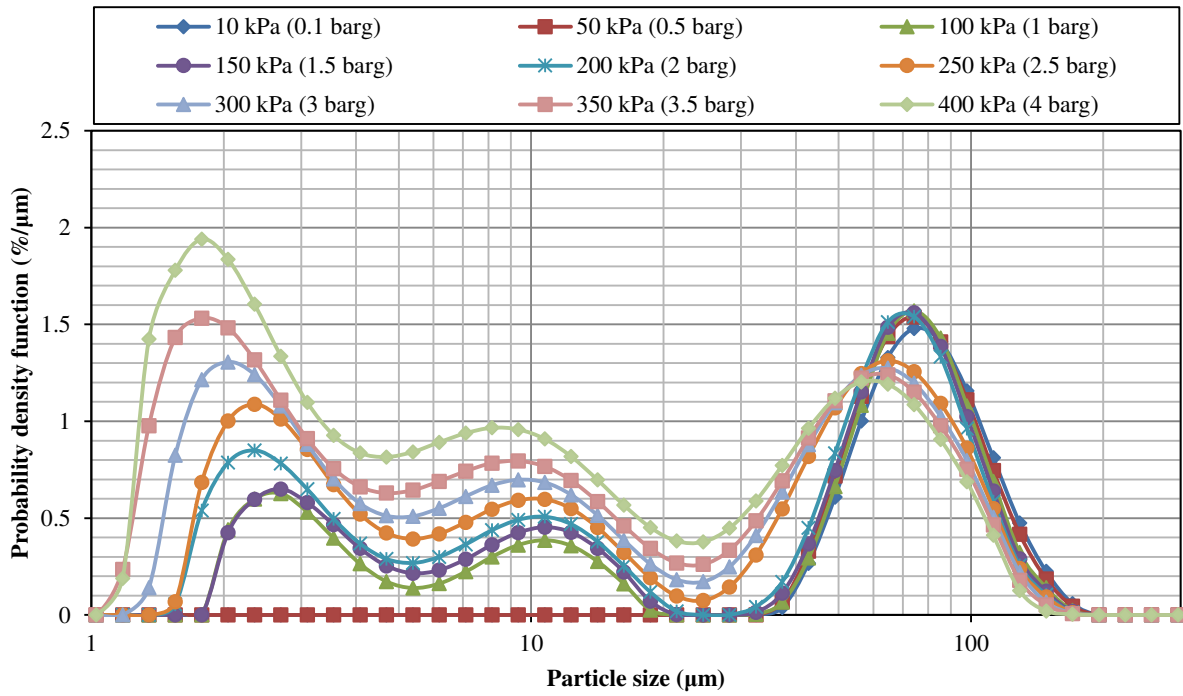


Figure a6: Shift in size distribution of 80-90 μm of α -lactose monohydrate at different nozzle air pressures

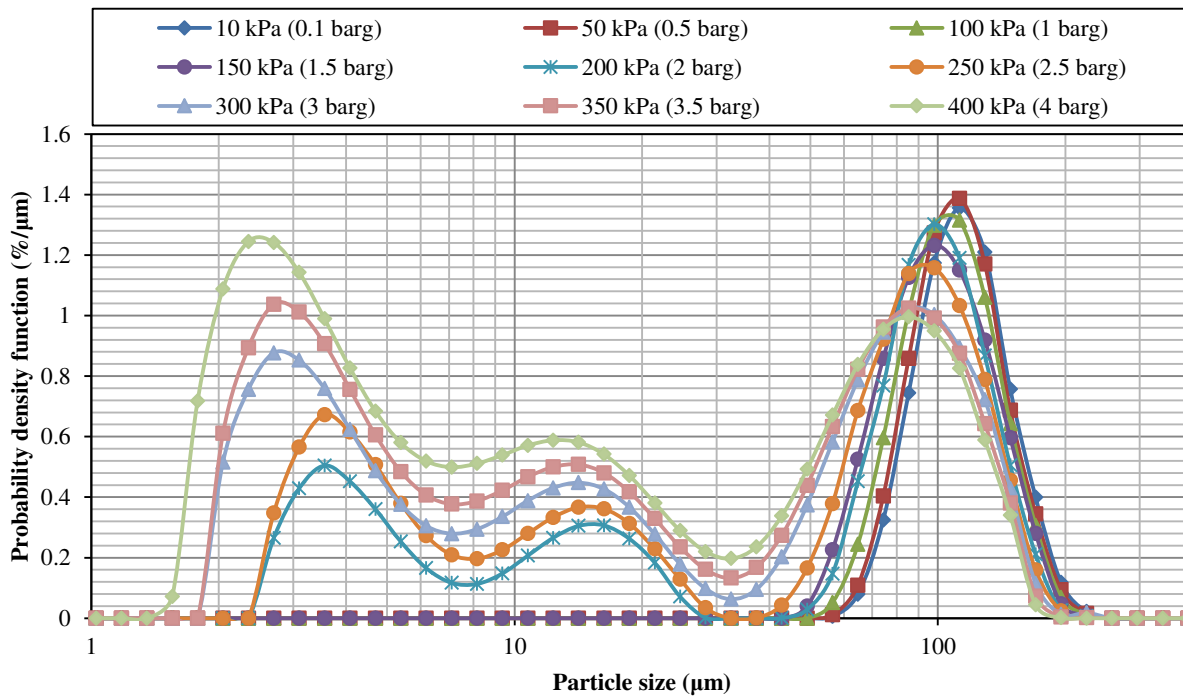


Figure a7: Shift in size distribution of 112-125 μm of α -lactose monohydrate at different nozzle air pressures

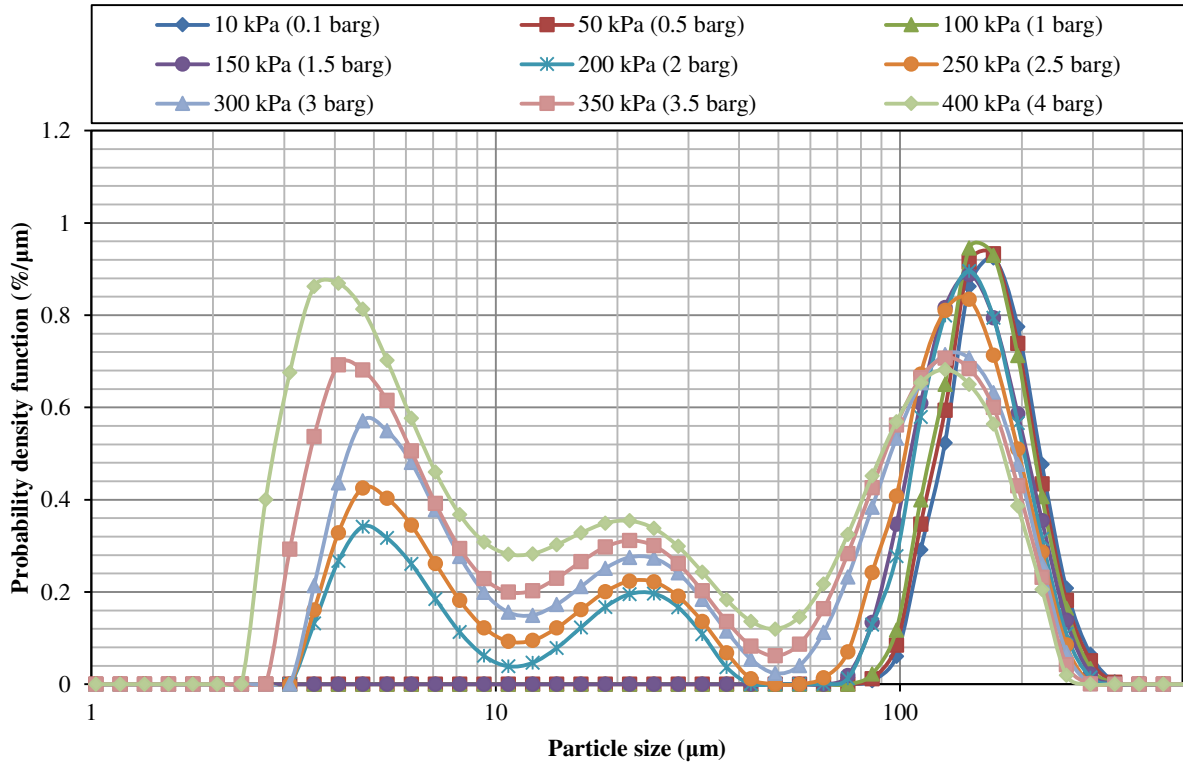


Figure a8: Shift in size distribution of 160-180 µm of α -lactose monohydrate at different nozzle air pressures